

# Pyrolysis of Lignin in Gas-Phase Isothermal and cw-CO<sub>2</sub> Laser Powered Non-Isothermal Reactors

Lavrent Khachatryan,\*\*,†,‡© Mohamad Barekati-Goudarzi,<sup>§</sup> David Kekejian, Gustavo Aguilar, Rubik Asatryan,<sup>#©</sup> George G. Stanley,<sup>†©</sup> and Dorin Boldor\*,†,§

Supporting Information

ABSTRACT: Pyrolysis of lignin in the gas-phase using "wall-less" and cw-IR CO2 laser powered homogeneous pyrolysis (LPHP) non-isothermal and continuous droplet evaporation (CDE) isothermal reactors has been performed. Hydrolytic lignin was dissolved in an acetone/water (9:1) mixture and dispersed into LPHP and CDE reactors using a constant output atomizing device and a syringe pump, respectively. Large differences in gas phase depolymerization of lignin have been seen in both reactors. The temperature distribution in the LPHP reactor was evaluated by thermocouple measurements and validated by the method of "chemical thermometer" and COMSOL Multiphysics simulations. The gas phase delivery of lignin into the hot zone of the LPHP reactor under "wall-less" conditions led to the breakdown of lignin into paramagnetic fragments that deposited onto the cell walls, which were studied by electron paramagnetic resonance spectroscopy. Phenolics were not detected at all in the LPHP reactor. However, major phenolics (phenol(s), guaiacol(s), syringol(s)) were detected in the CDE reactor. At laser powers higher than 20 W and a high initial concentration of dispersed lignin (5 g/L), an intensification of demethoxylation reactions of phenolics by concomitant alkylation of aromatic rings along with the expulsion of CO from phenoxy rings (to account for formation of indenes and naphtalenes) was achieved in the LPHP reactor when a prepyrolyzed mixture from the CDE reactor entered the LPHP reactor. The yields of qualified biofuel products such as styrene, different alkyl benzenes, and surrogate fuels of diesel such as indene, 1,2-dihydro naphthalene, naphthalene, and other derivatives were detected in the LPHP reactor with decreasing amounts of phenolics. These results represent valuable observations about the primary mechanism of lignin depolymerization.

# 1. INTRODUCTION

Natural resources such as crude oil and natural gas are the main sources for the production of conventional fuels and a wide variety of chemicals, but these feedstocks will eventually become limited. Biomass is a biorenewable and potentially carbon-neutral source that offers an alternative to crude oil and natural gas. Lignin is a major component of most biomass that can serve as a promising basic material for the production of aromatic compounds (phenolics) with a high added value. Remarkably, lignin is the only renewable natural resource of aromatic compounds.

Lignin, however, is challenging to process, and the pyrolysis of lignin to discrete aromatics still needs further development to make its utilization economically viable. Bio-oils can be produced from the pyrolysis of lignin, but the composition and quality are highly dependent on the conditions used. The resulting bio-oil can be upgraded in a number of ways (physically, chemically, and catalytically) to high quality biofuels and chemicals.<sup>3</sup>

1.1. Outlines of Lignin Pyrolysis. Thermogravimetric analysis of various lignin samples indicated the primary pyrolysis of lignin occurs between 200 and 400 °C, with the highest degradation rates achieved at ~380-400 °C.<sup>4,5</sup> The first stage of lignin decomposition, which occurs between 120 and 200 °C, can be called prepyrolysis and is mainly composed of dehydration reactions. Then, between 200 and 400 °C cleavages of  $\alpha$ - and  $\beta$ -alkyl-aryl ether bonds occur. These processes are accompanied by several competing, bondcleavage reactions at different temperatures depending on the bond energies.8 The most frequently studied reaction is the thermal scission of the weakest  $\alpha$ - and  $\beta$ -alkyl-aryl ether bonds because of their prominent role in lignin chemistry. 6-10 The cleavage of the ether-linkages in lignin leads to depolymerization of the lignin macromolecule, and formation of various lower molecular weight products with ether linkages. 11 The

Received: September 20, 2018 Revised: November 12, 2018

Published: November 14, 2018



<sup>†</sup>Department of Chemistry and <sup>||</sup>Departments of Physics and Astronomy, Louisiana State University, Baton Rouge, Louisiana 70803, United States

<sup>\*</sup>Department of Power Engineering, University Politehnica of Bucharest, Bucharest, Romania

SDepartment of Biological & Agricultural Engineering, Louisiana State University and LSU AgCenter, Baton Rouge, Louisiana 70803, United States

 $<sup>^{\</sup>perp}$ Adaptive Phage Therapeutics, 22 Firstfield Road Ste.125, Gaithersburg, Maryland 20878, United States

Department of Chemical and Biological Engineering, University at Buffalo, The State University of New York, Buffalo, New York 14260, United States

final stage of decomposition at higher temperatures (>400 °C) involves aliphatic side chains and methoxy groups splitting off from the aromatic rings, but at this point the decomposition chemistry becomes more complex with secondary and unwanted decomposition reactions taking place. Shorter pyrolysis times and higher temperatures (fast pyrolysis) are advantageous in obtaining higher liquid product yields and to decrease the generally unwanted char formation.

Another important issue is the product distribution from lignin pyrolysis, which is, to some extent, dependent on the nature and condition of the reactor walls as well as the surface of the lignin residue-char. The reactor wall and char surface can act as an autocatalyst for secondary tar reactions (STRs): cracking, (re)polymerization, and condensation during pyrolysis. <sup>14</sup>

1.2. Gas-Phase Pyrolysis of Dispersed Lignin. Recently, an investigation of lignin pyrolysis dispersed in the gas phase using a tubular reactor, abbreviated as the continuous droplet evaporation (CDE) system, has been reported. 15 The majority of interferences occurring naturally in solid phase pyrolysis, namely, mass-transfer limitations on polar and higher molecular mass compounds, the influence of surface area on the yields and kinetics for nascent compounds from pyrolysis of lignin, variation of pyrolysis rate with sample size and thickness, and the unknown character of reactions occurring in solid phase, were diminished. Hydrolytic lignin (HL) was dispersed into the gas phase up to the molecular size level, and the process of depolymerization in a "wall heated" CDE reactor, the gas-phase homogeneous conversion of lignin, was followed at a short residence time of 0.12 s with trace amounts of phenolics detected.

While the participation of the hot walls in the depolymerization of lignin in CDE reactor cannot be excluded, one can focus on the homogeneous gas-phase reactions by using an infrared laser powered homogeneous pyrolysis, or IR LPHP, reactor. This laser stimulated chemical pyrolysis method was successfully developed quite a while ago. 16-18 Briefly, in the IR LPHP reactor (often referred to as a "wall-less" reactor 16) energy is absorbed via a vibrational mode of the photosensitizer (mostly SF<sub>6</sub>), and rapidly converted into heat (translational energy) via efficient relaxation processes. 16,17 Energy is then transferred to the reagent molecules via collisions in much the same manner as in conventional pyrolysis. The IR LPHP technique generates a nonuniform temperature profile in the pyrolysis cell with a maximum near the cell axis and the cell walls remaining at close to room temperature. 17,19-22 The small dimensions aid in the rapid establishment of a steady-state temperature distribution and redistribution of reactants and products in the cell due to elimination of the wall effects on the reactions. 18,23

The IR LPHP method favors reaction pathways not influenced by hot wall effects. We, therefore, anticipate a drastic redistribution of products from dispersed lignin pyrolysis in the gas phase due to shortened radical-chain reactions and fast quenching of these reactions from the hot to cold zones of the reactor. Markedly, new products are expected to be produced under the IR LPHP of lignin due to the diverse heating rates, temperature, and residence times in the specific "wall-less" hot zone of the reactor at the given power of irradiation of the laser.

#### 2. EXPERIMENTAL SECTION

**2.1. Materials.** Hydrolytic lignin (HL) was supplied from Sigma-Aldrich (a discontinued product, #37-107-6). The weight percent ratio of C/H/O equals 76:6:18, and low molecular oligomers with a molecular weight below 500 Da are reported in ref 24. The majority of oligomers in HL correspond to dimers and trimers containing four oxygen atoms ( $C_{18}H_{18}O_4$ ) and six oxygen atoms ( $C_{27}H_{26}O_6$ ), respectively; the dimer ( $C_{18}H_{18}O_4$ ) is a major fraction in hydrolytic lignin. <sup>24</sup> Lignin was fractionated by filtration through molecular sieves (from mesh #60 to #120), and the fraction of  $\leq$ 125  $\mu$ m was used. The hydrolytic lignin was then well dissolved/sonicated for 30 min in acetone/water (9:1 volume ratio) mixture. <sup>2</sup> This solution was dispersed in the gas phase either by constant output TSI 3076 atomizer (COA), section 3.3, or continuous droplet evaporation using a syringe pump (section 3.4).

2.2. IR LPHP "Wall-less" Reactor. Experimental Design. A schematic of the IR LPHP reactor in flow condition is shown in Figure 1. The reactor is a Pyrex glass tube (i.d. = 20 mm, length = 10

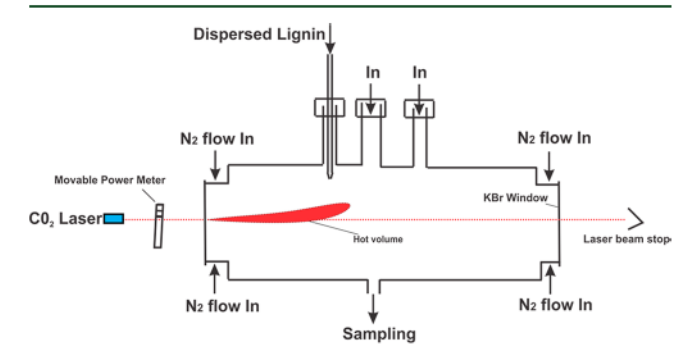


Figure 1. Schematic diagram of lignin laser powered homogeneous pyrolysis (LPHP) flow reactor.

cm) fitted from the both sides with KBr windows, highly transparent to the  $\rm CO_2$  laser irradiation (10.6  $\mu$ m). To avoid moisture's destructive effect on the hygroscopic window material as well as deposition of expected heavy intermediates from HL pyrolysis on the surfaces of both windows, they were protected by direct flow of  $\rm N_2$  through the reaction cell close to the windows, Figure 1. A cylindrical reactor without outlets could be used for static measurements. Other modified versions of the LPHP reactor are represented in Figures S1 and S7a, Supporting Information.

Concerning SF<sub>6</sub> as a sensitizer, it has a relatively fast vibration—translation relaxation time  $\sim 10^{-5}$  s at 1000 K and 1 atm total pressure. The absorbed laser energy is rapidly transferred to the ambient gas and reactants in that gas. An important characteristic of SF<sub>6</sub> is its general nonreactivity; it does not pyrolyze significantly below 1350 °C. The sense of the sense

The secondary tar-forming reactions will be limited in the LPHP reactor because of a sharp temperature drop on the border of the hot volume reaction zone and the corresponding drastic decrease of chain propagation reaction rates (vide infra). In other words, the extremely pronounced temperature decrease from the central reactor axis to the LPHP reactor wall may have a quite different effect on the various reaction steps than in a conventional heated tube reactor, as has been shown in earlier publications.  $^{21,23,25-30}$ 

- **2.3.** IR cw-CO<sub>2</sub> Laser. For the irradiation experiments, a continuous wave cw-CO<sub>2</sub> laser was used at the P (20) line of the  $00^{\circ}1 \rightarrow 10^{\circ}0$  transition (10.59  $\mu$ m) with an output of up to 40 W (Synrad Firestar CO<sub>2</sub> laser, FSV40KWD). The laser beam (o.d.  $\approx$  2.5 mm) in some experiments was focused (Ge lens, focal length 10 cm) behind the reactor window at different distances from the entry window as necessary.
- **2.4. CDE Reactor.** The details of operation for the CDE reactor were described elsewhere. <sup>15</sup> Briefly, the CDE reactor was interfaced with the syringe pump to deliver lignin dissolved in an acetone/water mixture (9:1), Figure 2. The solution was injected into a preferably

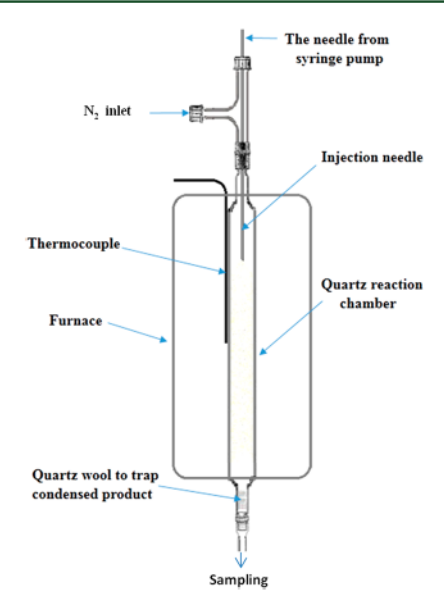


Figure 2. Schematic diagram of lignin continuous droplet evaporation (CDE) reactor.

high temperature area ( $\sim$ 250 °C) in a quartz reactor with i.d. = 12 mm and length = 14 cm. Pure N<sub>2</sub> gas with a flow rate of 1000 mL/min was used to carry the evaporated solvent with lignin dispersed particles through the reactor chamber which was heated using a conventional furnace.

The pyrolysis products from either LPHP or CDE reactors were trapped by dichloromethane in an impinger attached to the sampling port at 0  $^{\circ}$ C.

2.5. Thermocouple Measurements in LPHP Reactor. The measurement of the temperature distribution in the LPHP reactor is a complex problem, involving many factors reviewed thoroughly in ref 22.

The direct temperature measurements were performed using two K type thermocouples (o.d. = 0.001 in.); one was mounted at the inlet of LPHR reactor close to the wall, and the other was moved to the center of the reactor by increments of one millimeter, Figure S1, to define a temperature profile of the reactor cross-section. The temperatures closest to the laser beam (~8 mm from the wall) in a

static LPHP reactor reach 400 and 600 °C at laser powers of 6.6 and 10.8 W, respectively (Figure S2a). The temperature distribution close to the walls is much cooler at 100 and 120 °C under the same conditions (Figure S2b). The drastic change of temperature from the hot zone center to the cool walls means that pyrolysis reactions mostly occur in the central part of the LPHP reactor under strongly homogeneous conditions. Note that the hot volume schematically presented in Figure 1 occupies the axial region of the cell and may be extended almost to the back window by variation of  $N_2/SF_6$  ratio and the pressure inside the reactor. <sup>22</sup>

Similar temperature distributions have been mapped for the flow LPHP reactor depending on the flowing direction, flow rate, and thermocouple position, Figures S3 and S4. The thermocouple measurements have shown nonisothermal temperature distributions at given conditions.

### 3. RESULTS AND DISCUSSION

Since the direct measurement of temperature inside the laser beam using a thermocouple cannot be precise (because of the high rate of dissipation of energy through the thermocouple material), the method known as "chemical thermometer" was applied to approximate the temperature in the laser-heated hot zone.

**3.1. Chemical Thermometer.** Chemical thermometer, a technique pioneered by Shaub and Bauer, <sup>17</sup> was used for temperature measurements in a static LPHP reactor. In this method, the reaction under study is compared with one of the known characteristics of a reference material in the same pyrolysis cell. <sup>17,18,20,21,31</sup> The "chemical thermometer" approach measures spatially averaged temperatures and in general outcomes with self-consistent results. <sup>17,20</sup> As it has been shown in early publications at reactant pressures above 100 Torr, the molecular collision rate is sufficient to effectively thermalize the system, especially in gas phase dissociations and reactions induced by CW IR CO<sub>2</sub> laser. <sup>18,31</sup> All temperature measurements have indicated that the velocity distribution and temperature usually become steady-state in a few milliseconds, which is short compared with reaction times (seconds). <sup>17,22,32</sup>

A mixture of 1.6 Torr isopropyl bromide (IPB) and 8.7 Torr  $SF_6$  balanced by  $N_2$  gas up to 1 atm was subjected to  $CO_2$  laser irradiation for maximum temperature measurements at an

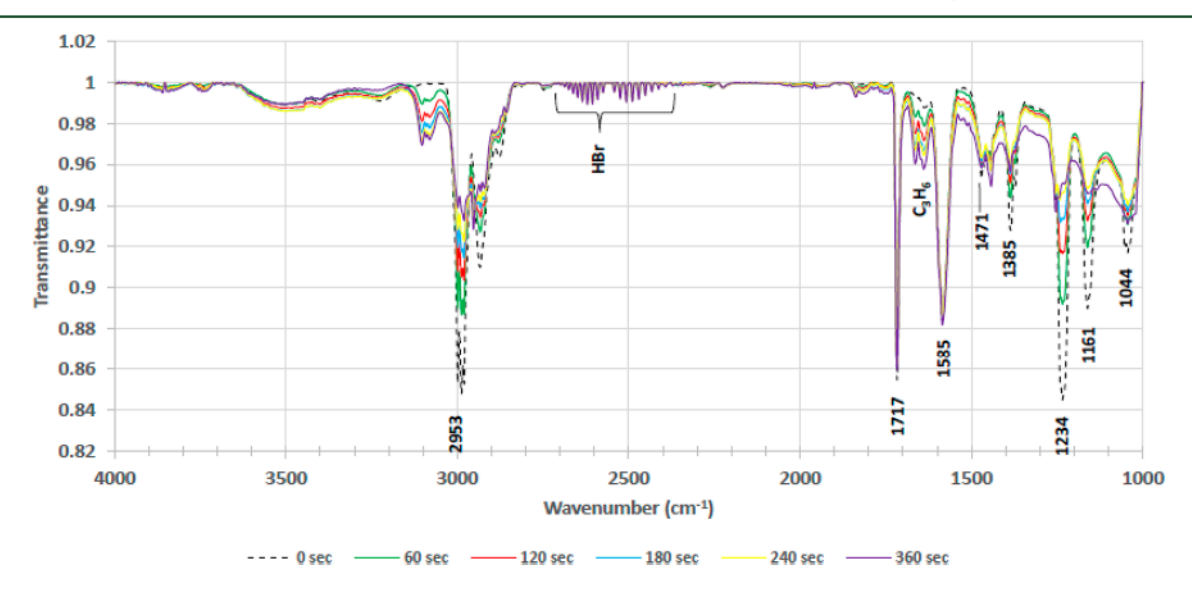


Figure 3. FTIR spectra of IPB (characteristic IR bands at 2953, 1385, 1234, 1161, 1044 cm $^{-1}$ ) and products (HBr from 2250 to 2750 cm $^{-1}$ ; C<sub>3</sub>H<sub>6</sub> between IR bands of SF<sub>6</sub> - 1585 and 1717 cm $^{-1}$  and higher than the 3000 cm $^{-1}$  region) from LPHP of IPB in static cell at CO<sub>2</sub> laser power of 6.7 W and time exposure from 0 to 360 s.

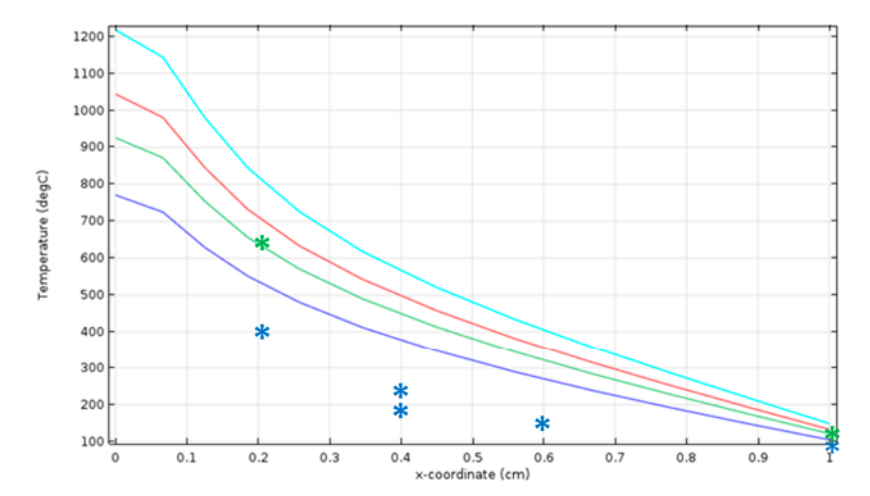


Figure 4. Calculated temperature distribution from the center of the laser beam toward the upper wall of the reactor at Z=2.2 cm from the entry window and laser power: blue line -6.6 W, green line -10.8 W, red line -15 W, cyan line -22 W. Asterisks are experimental measurements at given distances from the center of laser beam (X-coordinate) - data from Figures S2 and 3. Mixture content in the reactor -8.7 Torr SF<sub>6</sub> balanced by N<sub>2</sub> gas to 1 atm in static LPHP reactor.

incident laser power of 6.6 W. The Fourier transform infrared spectra of the products of laser powered pyrolysis of IPB are represented in Figure 3. The diminution of the integrated area of characteristic line of IPB at 1234 cm $^{-1}$  and formation one of the major products, HBr, in the region of 2250–2750 cm $^{-1}$  (Figure 3) are depicted in Figure S5 by yellow and blue lines, respectively. A typical first order decay curve for the line at 1234 cm $^{-1}$  is overlaid in Figure S5a–c (dotted lines) from which an average value for the apparent first order reaction rate constant of decomposition of IPB, 0.0063 s $^{-1}$ , was derived. This value was used for estimation of the temperature in the hot zone reaction volume.

The apparent rate constant  $(k_{\rm eff})$  for the first order decomposition reactions under non-isothermal conditions in LPHP reactor is averaged over the reaction cell volume as

$$k_{\text{eff}} = \frac{\int k_0 \exp\left[-\frac{E}{RT(\nu)}\right] dV/T(\nu)}{\int dV/T(\nu)}$$
(1)

where  $T(\nu)$  is the volume  $(\nu)$  temperature distribution in the vessel,  $k_0 \exp\left(-\left[\frac{R}{RT(\nu)}\right]\right)$  is the real rate constant for given reaction. Because the temperature gradient in the IR cell is large (Figure S2), therefore, the eq 1 for the reactions with high activation energies of decomposition  $(\sim\!E/RT>10)$  can be approximated as

$$k_{\text{eff}} = \frac{V_{\text{eff}}}{V_0} k_0 \exp{-\left[\frac{E}{RT \text{max}}\right]}$$
 (2)

where  $V_{\rm eff}$  is the volume of hot zone limited by laser beam volume in the center of the reactor, and  $V_{\rm o}$  is IR cell volume. In a number of research studies, the ratio  $V_{\rm eff}/V_{\rm o}$  was estimated in the range of  $10^{-3}$  to  $10^{-1}$  by assuming that the monomolecular decompositions of organics occur in the kinetic regime.  $^{17,18,20-22,31,33}$  With this large discrepancy of the ratio  $V_{\rm eff}/V_{\rm o}$  and based on our experimental data for apparent rate constant of 0.0063 s<sup>-1</sup> for the IPB LPHP reaction, the  $T_{\rm max}$  estimation was calculated to be changed from 823 K (at  $V_{\rm eff}/V_{\rm o} = 10^{-3}$ ) to 703 K ( $V_{\rm eff}/V_{\rm o} = 10^{-1}$ ). A well-known value of  $10^{13.8}$  exp (-47500 cal/mol/RT) s<sup>-1</sup> for the real rate constant of IPB decomposition was chosen  $^{34}$  from shock tubes (similar

to "wall-less" reactors) that have little or no pressure dependence. Therefore, a suitable temperature for lignin pyrolysis can be determined using this methodology starting at a laser power of 6.6 W and higher at our experimental conditions (i.e., flow rate, hot volume size, and location).

3.2. A Theoretical/Numerical Prediction of the Temperature in the Hot Zone. To verify the value of measured maximum temperature in the laser beam a theoretical/numerical calculation was initiated which solves the heat eq 3 in cylindrical coordinates using COMSOL Multiphysics (heat transfer module).

$$\rho C_p \frac{\partial T}{\partial t} + k \nabla^2 T = -\frac{d\mathbf{I}}{d\mathbf{z}} \tag{3}$$

where  $\rho$  is the density,  $C_p$  is the heat capacity at a constant pressure, k is the thermal conductivity, T denotes the temperature for which the equation is solved for, t is time, and I is the intensity of the laser beam propagating in the mixture as a function of z, the length of the reactor.

The static LPHP reactor is modeled as a cylinder in COMSOL with a diameter of 20 mm and a length of 10 cm. We assume the laser beam to have a Gaussian profile in the following way (eq 4)

$$I = 0.9I_0 \exp\left(-\frac{r^2}{\sigma^2}\right) \tag{4}$$

where r is the radial coordinate,  $\sigma = 1.25$  mm denotes radius of the laser beam, 0.9 is the transmission coefficient of the reactor wall, and  $I_0$  is the initial laser beam intensity used in the experiment and is related to the laser power in the following way (eq 5), where P is the laser power.

$$I_0 = \frac{P}{\pi \sigma^2} \tag{5}$$

Dissipation of the heat through the window is modeled into COMSOL in the form of Stefan-Boltzmann gray body radiation expressed by  $\varepsilon(T)$   $\sigma_s(T^4 - T_{amb}^4)$ , where  $\varepsilon(T)$  is the gray body (glass window) emission coefficient (equals 0.88-0.91, which is a function of the temperature and the thickness of the glass<sup>35</sup>);  $\sigma_s$  is the Stefan-Boltzmann constant,

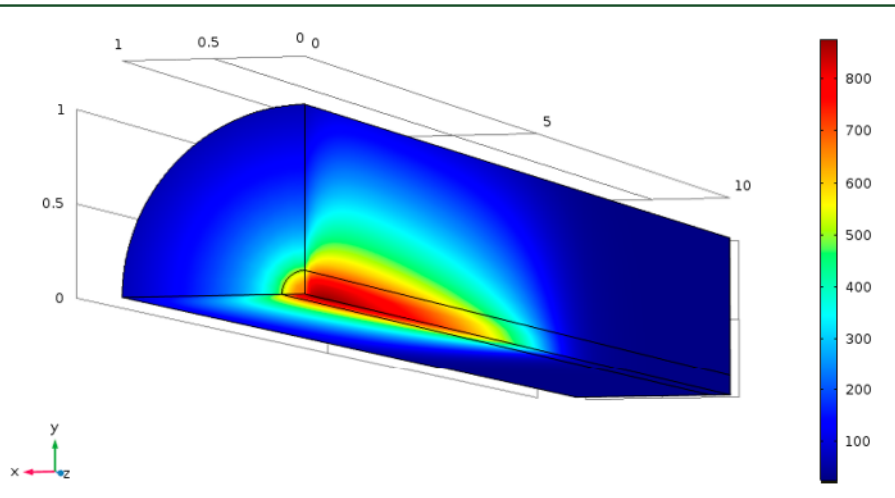


Figure 5. COMSOL prediction of the "hot zone". 1/4th part of the hot zone in X, Y, Z coordinates (3D picture) is presented at 6.6 W laser power irradiation in coaxial static reactor (i.d. = 20 mm, length 100 mm) and mixture content -8.7 Torr SF<sub>6</sub> balanced by N<sub>2</sub> gas to 1 atm.

and  $T_{amb}$  is the ambient temperature which is taken to be 300 K.

Since the heating of the gas is due to absorption of the laser energy by SF<sub>6</sub> molecules, the Beer–Lambert law  $I(z) = I_0 e^{-\mu(T)z}$  was used to describe the drop of the laser intensity toward the length of the LPHP reactor. Due to high transparency of the nitrogen in the spectral region higher than 0.1  $\mu$ m (the absorption coefficient  $\approx 0.01 \, \text{Torr}^{-1} \, \text{cm}^{-1}$  at 0.16  $\mu$ m<sup>36</sup>), the laser absorption by N<sub>2</sub> is negligible and the heat source in LPHP reactor is the SF<sub>6</sub> gas absorbing laser energy at a high absorption coefficient of 0.55  $\, \text{Torr}^{-1} \, \text{cm}^{-1}$  at room temperature.<sup>37</sup> Note that the temperature dependence of the absorption coefficient of SF<sub>6</sub> has been included in COMSOL calculations based on early experimental measurements.<sup>38</sup>

COMSOL Simulation Results. The temperature distribution profiles predicted by COMSOL at different powers of the laser from the center of laser beam (X = 0.0 mm) toward the upper wall at distance of 2.2 cm from entry window are depicted in Figure 4.

The calculation yields a realistic agreement between the experiment and simulation on the wall of the LPHP reactor (blue and green asterisks at X = 1 cm from the center of laser beam and laser power of 6.6. and 10.8 W, respectively) and almost the same value of 630 °C on the border of laser beam (green line and green asterisks at X = 2 mm, laser power 10.8 W), while a difference ~130 °C was detected between calculation (530 °C) and measurement (400 °C) at a laser power of 6.6.W (blue line and blue asterisks, Figure 3). A similar discrepancy has been seen between the measured and simulated temperature profiles at X = 4 mm and 6 mm, Figure 4. Consideration of convection heat transfer phenomenon may yield more accurate simulation values. The experimentally measured temperature profile is steeper (asterisks in Figure 4) than the COMSOL prediction (blue line at 6.6 W), supporting our contention that the LPHP reactor is functioning in a "wallless" mode.

A pictorial presentation of the hot volume predicted by COMSOL at laser power of 6.6.W is presented in Figure 5. The length of the hot volume is extended up to 3–4 cm from the entry window, Figure 5, at  $V_{\rm eff} \approx 0.2~{\rm cm}^3$  and  $V_{\rm eff}/V_{\rm o} = 5.2 \times 10^{-3}$ , which is compatible with the lower value of  $V_{\rm eff}/V_{\rm o} = 10^{-3}$  for the chemical thermometer measurements that give a temperature of 823 K in the hot volume (section 3.1). In fact,

the average simulated temperature of  $\sim 903$  K for the hot volume (Figures 4 and 5) is reasonable close to the value extracted from "chemical thermometer" measurements (823 K).

Therefore, the COMSOL calculations can be used to map temperature distributions in different LPHP reactors (static or dynamic) depending on CO<sub>2</sub> laser power (see Figure S6), SF<sub>6</sub> sensitizer concentration, total pressure in the reactor, flow rates, etc.

3.3. Laser Powered Homogeneous Pyrolysis of HL in the Gas Phase at Non-Isothermal Conditions. A commercially available TSI 3076 Constant Output atomizer was coupled with the modified LPHP reactor (Figure S7) to avoid possible agglomeration of HL in the gas phase. The atomizer improves the delivery of dispersed lignin into the gas phase. This atomizer has been successfully used to disperse nonsoluble sub-micrometer particles, such as carbon black. The aerosol formed from carbon black consists mainly of primary particles—the agglomerates that are fused together by the carbon black manufacturing process—and the level of agglomerates was very low.

The atomization of lignin into the gas phase and the transport through the LPHP reactor revealed detection of intrinsic components of initial lignin by GC-MS as 2,3-dihydrobenzofuran (peak #1), 4-vinyl guaiacol (peak #2), and a major component at 26.45 min (peak #3 identified tentatively in ref 15 as a O<sub>4</sub> dimer - C<sub>17</sub>H<sub>16</sub>O<sub>4</sub>, Figure 6a. As the laser power was applied, the intensity of intrinsic compounds was dropped continuously, and for instance, 4-vinyl guaiacol (2-methoxy-4-vinylphenol) and 2,3-dihydrobenzofuran were destroyed completely at a laser power of 14.5 W, Figure 6b. The intensity of the dominant peak at 26.45 min (peak #3, Figure 6a) dropped by a factor of 4 at the same power of 14.5 W (Figure 6b) and disappeared at higher than 22 W power: no phenolics were detected in the entire region of powered pyrolysis of dispersed lignin up to 40 W.

Instead, a brown deposit was observed on the walls of an inner cylinder located inside the LPHP reactor at a wide range of laser powers from 14 W to 40 W (Figure S7). The experiments show a high radical content of the deposit on the walls removed by quartz wool and subjected to EPR analysis, Figure S7. The normalized intensity of radicals (spins per gram) of brown deposit is higher by a factor of 7 compared to the initial radical content of lignin used, which is known to be

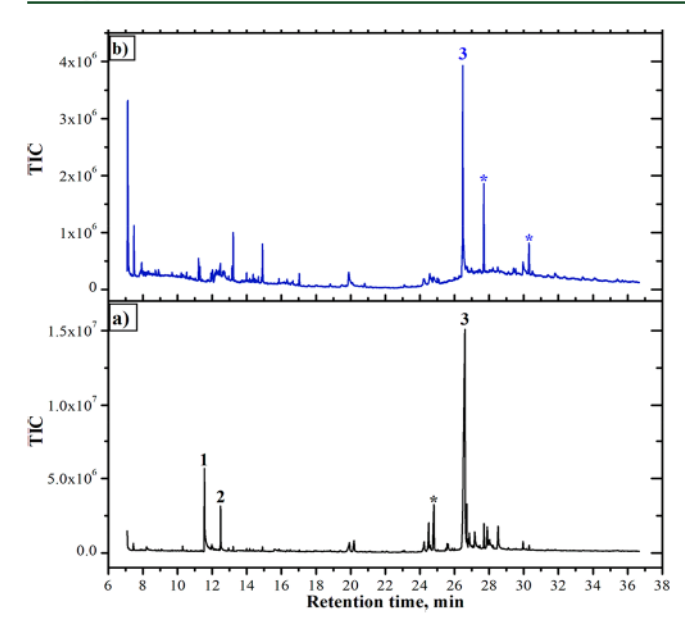


Figure 6. GC-MS data before (a) and after (b) pyrolysis of dispersed HL into the LPHP reactor at a CO<sub>2</sub> laser power of 14.5 W; 1–2, 3-dihydrobenzofuran; 2-4-vinyl guaiacol; 3 a dimer with molecular weight of 284 Da. 15 Peaks assigned by asterisks were not identified.

on the order of ~10<sup>17</sup> spins/g.<sup>40</sup> This is a valuable experimental observation demonstrating that one of the primary processes of depolymerization may occur through the fragmentation of HL by formation of oligomer radicals. Because of the steep temperature zone in the center of the LPHP reactor, these fragments quickly leave the hot zone and quench or stabilize in the cold areas of the reactor. Additional research is needed to identify the origin of these intermediate products from primary pyrolysis of lignin.

3.4. Pyrolysis of HL in CDE Reactor at Isothermal Conditions; Products Distribution. Preliminary results concerning dispersed lignin pyrolysis in the gas phase in a CDE reactor (section 2.4) were reported recently. 15 A distribution of major grouped components, such as guaiacol and derivatives (GUA), phenol and derivatives (PHE), syringol and derivatives (SYR), 2,3-dihydrobenzofuran (BEF), and others from pyrolysis of HL in conventional and CDE reactors are illustrated in Figure 7 and inset pictures, respectively. The number of grouped products and their distribution in the CDE reactor differs greatly from the results of a regular, fractional pyrolysis of lignin. For example, if the ratio of major phenolics GUA/SYR is equal to ~1.7:1.0 (Figure 7), then the same ratio is changed to an average of 3:1 in the CDE reactor, Figure 7 (inset). The typical ratio between GUA/SYR ranges from 1.1 to 2.2 for different natural lignins. 41 In fact, specific conditions have been achieved in the CDE reactor that change the GUA/SYR ratio toward formation of guaiacol group products with a large dominance of 4-vinyl guaiacol. Surprisingly, high yields of 2,3-dihydrobenzofuran (BEF) were detected from HL pyrolysis in the CDE reactor,

The high yields of guaiacol compounds are due to the specific environment established in the CDE reactor in the gas phase. The secondary tar reactions (STR), especially radicalchain reactions, providing further degradation of the intermediate products are minimized due to the fast flow and contactless conditions of released products with the

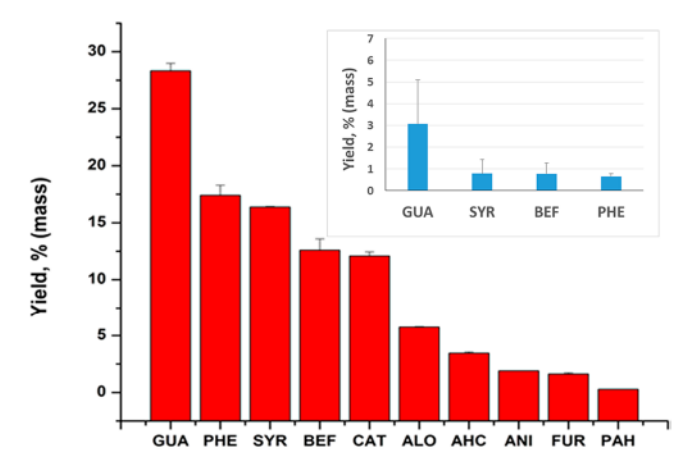


Figure 7. Distributions of major grouped products from HL pyrolysis in a tubular, fractional pyrolysis (red bars) and CDE (inset) reactors. The experimental measurements are an average from two replicates. The abbreviations of the grouped products (and derivatives): GUA - guaiacols; PHE - phenolics; SYR - syringols; BEF - 2,3-dihydrobenzofuran; CAT - catechols; ALO - aliphatic oxycompounds; ANI - anisols; FUR - furans; PAH - aromatic hydrocarbons.

surface of the char residue. The relatively high yields of GUA compounds indicate, on the other hand, that the number of the phenolics in fractional/conventional pyrolysis form through the secondary reactions of guaiacols demonstrated experimentally<sup>42–44</sup> and theoretically.<sup>45,46</sup> For instance, the well-known product of catechol, CAT (ref Figure 7), that forms in further pyrolysis of guaiacol as a major product<sup>43,47</sup> is practically missing in the CDE reactor (Figure 7, inset).

3.5. Pyrolysis of HL in Coupled CDE + LPHP Reactors System. The LPHP and CDE reactors described above were coupled to activate the pyrolysis of HL in the LPHP reactor, Figure S8a and b, respectively. The evaporated HL/acetone solution in the gas phase was mixed with SF<sub>6</sub> containing N<sub>2</sub> carrier gas flow (volumetric percentage of SF<sub>6</sub> from 1.13 to 6.5% depending on experimental conditions), Figure S8b. Then the flow at a residence time of 0.12 s in the CDE reactor with a content of ~ 85% unreacted lignin and number of known products (guaiacol, 2,3-dihydrobenzofuran, 4-vinyl guaiacol, syringol, and a dimer with molecular weight of 284 Da<sup>15</sup>) enters the LPHP reactor, Figure S8a. This prepyrolyzed mixture was subjected IR CO2 laser irradiation at a power of 16 W. The results are shown in Figure 8a,b; a distinct change of the dimer yield by a factor of 3-4 was detected in the LPHP reactor (#8 product in Figure 8b), with no significant influence on the formation rate of phenolics.

The short residence and reaction time can be one of the reasons for low conversion of lignin in LPHP reactor at the current conditions. Indeed, the residence time through the hot volume of  $\sim 0.038$  cm<sup>3</sup>, or 3.8 cm<sup>3</sup> (at  $V_{\rm eff}/V_o = 10^{-3} - 10^{-1}$ ,  $V_{\rm eff}$  can be varied from 0.038 cm<sup>3</sup> to 3.8 cm<sup>3</sup> at total volume of 38 cm<sup>3</sup>) is  $\leq 0.6$  ms or  $\leq 63$  ms, respectively, at an average temperature of hot volume  $\sim 763$  K and a carrier gas flow rate of 1000 mL/min.

The residence time may be even less because of the horizontal location of the hot volume while the flow crosses vertically through part of the hot volume. A heating time of 17 ms is calculated for a spherical biomass particle with a radius of 50  $\mu$ m to go from an ambient temperature to  $\sim$ 773 K during conventional fast pyrolysis. Presumably, very small particles

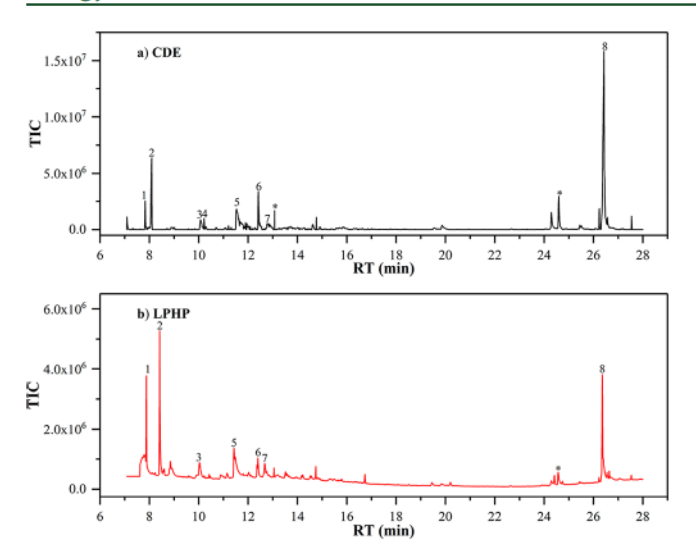


Figure 8. (a) The products from partial pyrolysis of dispersed lignin in the CDE reactor in the gas phase at 500 °C: 1. 1-methylethylbenzene ( $C_9H_{12}$ ); 2. 2,5-hexanedione ( $C_6H_{10}O_2$ ); 3. guaiacol ( $C_7H_8O_2$ ); 4. carveol ( $C_{10}H_{16}O$ ); 5. 2,3-dihydro benzofuran ( $C_8H_8O$ ); 6. 4-vinyl guaiacol ( $C_{10}H_{14}O$ ); 7. syringol ( $C_8H_{10}O_3$ ); 8. A dimer with molecular weight of 284 Da. <sup>15</sup> (b) The products distribution in LPHP reactor at ~16 W of laser power irradiation as the prepyrolyzed mixture from the CDE reactor enters LPHP reactor. Peaks assigned by asterisks were not identified.

of lignin with a size of  $0.5 \mu m^{49}$  will meet the conditions of fast heating from an ambient temperature in the range of milliseconds. Note that the amount of lignin passed through the hot volume in the LPHP reactor during 0.6 ms is on the order of micrograms ( $1.2 \mu g$  at concentration of initial lignin 1

g/L). The evidence that such a small amount is heated is the experimental fact of immediate deposition of depolymerized fragments of HL on the walls of the reactor.

Intensification of Demethoxylation Reactions in LPHP Reactor As Coupled with the CDE Reactor. To further intensify the conversion of HL in the LPHP reactor, the initial concentration of HL was increased along with a higher laser power and residence times through the hot volume, Figure S8a. A small CDE reactor (i.d. = 12 mm, length = 7 cm) was coupled with the LPHP reactor. The evolved products from HL prepyrolysis in the CDE reactor were subjected to further conversion in the LPHP reactor at initial concentration of HL 5 g/L, a feeding rate of 4 mL/h into the CDE reactor, and a laser power of 22 W in the LPHP reactor, Figure 9. The carrier gas flow was set at 420 mL/min with  $\sim$ 2.8% SF<sub>6</sub> in the N<sub>2</sub> gas. The lower flow rate was used for the smaller CDE reactor to maintain the same residence time of 0.12 s, while the residence time in the hot zone inside the LPHP reactor increases proportionally (almost 2.4 times).

In these circumstances, the number of phenolics generated from the CDE reactor (Figure 9a, Table 1) were converted into valuable aromatic fuels in the LPHP reactor—methylated benzenes, styrene, indene, naphthalene, and derivatives, Figure 9b, Table 2.

In fact, at the laser power of 22 W, a high initial concentration of dispersed lignin (5 g/L) and longer residence times in LPHP led to an intensification of the demethoxylation reactions of guaiacols, syringols (by concomitant alkylation of aromatic rings), along with the expulsion of CO from phenoxy rings.  $^{47,50,51}$ 

This scenario clearly shows that the temperature in the hot zone is higher than 550-600 °C (ref COMSOL prediction, Figure S6), which favors the above-mentioned and other

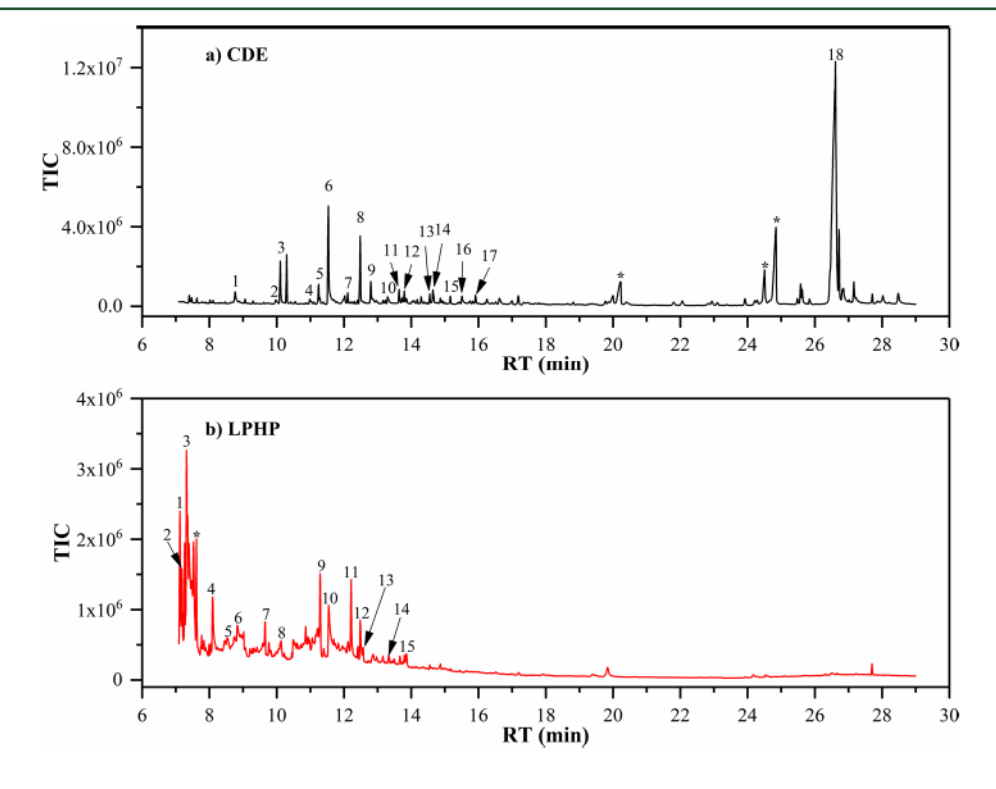


Figure 9. (a) Products distribution after pyrolysis of dispersed HL in the CDE reactor at 500 °C and 0.12 s residence time. (b) Products distribution in LPHP reactor at laser irradiation of 22 W as flow from the CDE reactor enters LPHP reactor. Peaks assigned by asterisks were not identified.

Table 1. Products Distribution from CDE Reactor, Figure 9a

Cpd	name	formula	RT	area	yield, mass, %
1	phenol	C <sub>6</sub> H <sub>6</sub> O	8.766	$1.96 \times 10^{6}$	$1.55 \times 10^{-1}$
2	phenol, 3-methyl-	$C_7H_8O$	9.977	$7.80 \times 10^{5}$	$6.16 \times 10^{-2}$
3	phenol, 2-methoxy-	$C_7H_8O_2$	10.106	$3.91 \times 10^{6}$	$2.82 \times 10^{-1}$
4	phenol, 3-ethyl-	$C_8H_{10}O$	10.985	$6.71 \times 10^{5}$	$5.30 \times 10^{-2}$
5	phenol, 2-methoxy-4-methyl-	$C_8H_{10}O_2$	11.25	$1.67 \times 10^{6}$	$1.21 \times 10^{-1}$
6	benzofuran, 2,3-dihydro-	$C_8H_8O$	11.539-11.698	$1.24 \times 10^{7}$	$9.18 \times 10^{-1}$
7	phenol, 4-ethyl-2-methoxy-	$C_9H_{12}O_2$	12.11	$9.61 \times 10^{5}$	$6.94 \times 10^{-2}$
8	2-methoxy-4-vinylphenol	$C_9H_{10}O_2$	12.486	$5.89 \times 10^{6}$	$2.14 \times 10$
9	phenol, 2,6-dimethoxy-	$C_8H_{10}O_3$	12.799-12.861	$2.97 \times 10^{6}$	$2.30 \times 10^{-1}$
10	vanillin	$C_8H_8O_3$	13.297	$1.13 \times 10^{6}$	
11	phenol, 4-methoxy-3-(methoxymethyl)-	$C_9H_{12}O_3$	13.641	$1.16 \times 10^{6}$	
12	phenol, 2,6-dimethoxy-	$C_8H_{10}O_3$	13.795	$9.22 \times 10^{5}$	$7.14 \times 10^{-2}$
13	phenol, 4-methoxy-3-(methoxymethyl)-	$C_9H_{12}O_3$	14.551	$5.97 \times 10^{5}$	
14	3-tert-butyl-4-hydroxyanisole	$C_{11}H_{16}O_2$	14.644	$1.58 \times 10^{6}$	$1.17 \times 10^{-2}$
15	5-tert-butylpyrogallol	$C_{10}H_{14}O_3$	15.16	$7.58 \times 10^{5}$	
16	benzaldehyde, 4-hydroxy-3,5-dimethoxy-	$C_9H_{10}O_4$	15.511	$1.30 \times 10^{6}$	
17	phenol, 2,6-dimethoxy-4-(2-propenyl)-	$C_{11}H_{14}O_3$	15.91	$1.02 \times 10^{6}$	
18	O <sub>4</sub> dimer		26.45	$6.68 \times 10^{07}$	

Table 2. Products Distribution from LPHP Reactor, Figure 9b

Cpd	name	formula	RT		yield, mass, %
1	benzene, 1,2-dimethyl-	$C_8H_{10}$	7.124	$3.83 \times 10^{6}$	0.26
2	benzene, ethynyl-	$C_8H_6$	7.179	$2.67 \times 10^6$	0.18
3	styrene	$C_8H_8$	7.32-7.529	$2.15 \times 10^{7}$	1.44
4	2,5-hexanedione	$C_6H_{10}O_2$	8.095	$5.67 \times 10^6$	
5	benzene, 1,3,5-trimethyl-	$C_9H_{12}$	8.458-8.532	$9.45 \times 10^{5}$	0.06
6	benzene, 1-propenyl-	$C_9H_{10}$	8.741-8.827	$9.46 \times 10^{5}$	0.06
7	1H-indene	$C_9H_8$	9.331-9.657	$2.27 \times 10^{6}$	
8	5,7-dodecadiyn-1,12-diol	$C_{12}H_{18}O_2$	10.106-10.13	$1.04 \times 10^{6}$	
9	naphthalene	$C_{10}H_{8}$	11.292	$1.45 \times 10^{6}$	
10	benzofuran, 2,3-dihydro-	$C_8H_8O$	11.545	$2.97 \times 10^{6}$	0.22
11	benzaldehyde, 4-methyl-	$C_8H_8O$	12.215	$1.67 \times 10^{6}$	
12	phenol, 2-(1,1-dimethylethyl)-	$C_{10}H_{14}O$	12.485	$1.10 \times 10^{6}$	0.87
13	naphthalene, 2-methyl-	$C_{11}H_{10}$	12.571	$3.15 \times 10^{5}$	
14	naphthalene, 1,5-dimethyl-	$C_{12}H_{12}$	13.328	$2.65 \times 10^{5}$	
15	benzenemethanol, 3-hydroxy- 5-methoxy-	$C_8H_{10}O_3$	13.666-13.795	$5.28 \times 10^{5}$	

secondary reactions. 42,43,52 The expulsion of CO from phenoxy rings that leads to formation of cyclopentadienyl radicals (and hydroxy-cyclopentadienyl from pyrolysis of guaiacol<sup>47</sup>) and their further recombination by formation of naphtalenes was experimentally established in isothermal reactors. 5350,51 Note that at a high laser power the dimer peak at 26.45 min from the CDE reactor, Figure 9a, is completely consumed in the LPHP reactor, Figure 9b. This results from the higher temperature and longer residence time in the hot zone, which enables a complete conversion of the dimer to products. Furthermore, the depolymerization of dispersed HL by formation of phenolic compounds, as flow from the CDE reactor enters the LPHP reactor, has not been seen at a high concentration of lignin as well.

# 4. CONCLUSIONS

Pyrolysis of hydrolytic lignin (HL) dispersed in the gas phase has been performed in cw-IR CO<sub>2</sub> laser powered homogeneous pyrolysis (LPHP) non-isothermal and continuous droplet evaporation (CDE) isothermal reactors. Large differences in the products distribution resulting from the gas phase depolymerization of HL have been seen in both reactors. The

gas phase delivery of HL into the hot zone area of the LPHP reactor coupled with an atomizer under wall-less conditions leads to the breakdown of HL into radicals and other fragments deposited on the cell walls of the reactor as validated by EPR measurements. No phenolics at all were detected under these strongly homogeneous pyrolysis conditions.

When the CDE and LPHP reactors were coupled and a prepyrolyzed reaction mixture from the CDE reactor entered the LPHP reactor, further conversion of the reaction mixture took place at laser powers higher than 20 W and high initial concentrations of dispersed lignin (5 g/L). An intensification of demethoxylation reactions of guaiacols, syringols (by concomitant alkylation of aromatic rings), along with the expulsion of CO from phenoxy rings (to form indenes, naphtalenes) was achieved in the LPHP system. Therefore, coupled CDE + LPHP reactors may be a promising tool for biomass pyrolysis toward selective production of valuable biooil components opening new reaction pathways of depolymerization of lignin not predicted or observed via conventional techniques.

The temperature distributions in the LPHP reactor were performed by thermocouple measurements and validated by the methods of "Chemical Thermometer" and COMSOL Multiphysics.

# ASSOCIATED CONTENT

## Supporting Information

The Supporting Information is available free of charge on the ACS Publications website at DOI: 10.1021/acs.energy-fuels.8b03312.

Temperature direct measurements outside of the laser beam in static and dynamic LPHP reactor (PDF)

#### AUTHOR INFORMATION

### **Corresponding Authors**

\*(L.K.) E-mail: Lkhach1@lsu.edu.

\*(D.B.) E-mail: DBoldor@agcenter.lsu.edu.

ORCID ©

Lavrent Khachatryan: 0000-0002-8067-7964 Rubik Asatryan: 0000-0003-1200-2727 George G. Stanley: 0000-0002-2834-7626

Notes

The authors declare no competing financial interest.

# ■ ACKNOWLEDGMENTS

This work was funded by National Science Foundation grant (No. 1330311). L.K. acknowledges Dr. Mengxia Xu from University of Nottingham Ningbo, China, for hydrolytic lignin conventional pyrolysis experiments. The authors acknowledge a partial support from NSF EPSCoR (OIA #1632854) and USDA-NIFA Hatch program (LAB #94146). Published with the approval of the Director of the Louisiana Agricultural Experiment Station as manuscript #2018-232-33372. This study was also partially supported by Romania's "Competitiveness Operational Programme 2014-2020", Priority Axis 1: Research, Technological Development and Innovation (RD&I) to Support Economic Competitiveness and Business Development, Action 1.1.4. Attracting high-level personnel from abroad in order to enhance the RD capacity, ID/Cod My SMIS: P\_37\_768/schita: 103651; Contract No. 39/ 02.09.2016.

#### REFERENCES

- (1) Dorrestijn, E.; Laarhoven, L. J.J.; Arends, I. W.C.E.; Mulder, P. The occurrence and reactivity of phenoxyl linkages in lignin and low rank coal. *J. Anal. Appl. Pyrolysis* 2000, 54, 153–192.
- (2) Nowakowski, D. J.; Bridgwater, A. V.; Elliott, D. C.; Meier, D.; de Wild, P. Lignin fast pyrolysis: Results from an international collaboration. *J. Anal. Appl. Pyrolysis* 2010, 88 (1), 53–72.
- (3) Bridgwater, A. V. Review of fast pyrolysis of biomass and product upgrading. *Biomass Bioenergy* 2012, 38, 68–94.
- (4) Jiang, Z. H.; Argyropoulos, D. S. Coupling P-31 NMR with the Mannich reaction for the quantitative analysis of lignin. *Can. J. Chem.* 1998, 76 (5), 612–622.
- (5) Ben, H. X.; Ragauskas, A. J. NMR Characterization of Pyrolysis Oils from Kraft Lignin. *Energy Fuels* 2011, 25 (5), 2322-2332.
- (6) Huang, J. B.; Liu, C.; Wu, D.; Tong, H.; Ren, L. R. Density functional theory studies on pyrolysis mechanism of beta-O-4 type lignin dimer model compound. *J. Anal. Appl. Pyrolysis* 2014, 109, 98–108.
- (7) Huang, J. B.; He, C.; Pan, G. Y.; Tong, H. A theoretical research on pyrolysis reactions mechanism of coumarone-contained lignin model compound. *Comput. Theor. Chem.* 2016, 1091, 92–98.

(8) Jakab, E.; Faix, O.; Till, F. Thermal decomposition of milled wood lignins studied by thermogravimetry mass spectrometry. *J. Anal. Appl. Pyrolysis* 1997, 40–41, 171–186.

(9) Kawamoto, H.; Ryoritani, M.; Saka, S. Different pyrolytic cleavage mechanisms of  $\beta$ -ether bond depending on the side-chain structure of lignin dimers. J. Anal. Appl. Pyrolysis 2008, 81 (1), 88–94.

- (10) Nakamura, T.; Kawamoto, H.; Saka, S. Pyrolysis behavior of Japanese cedar wood lignin studied with various model dimers. *J. Anal. Appl. Pyrolysis* 2008, 81 (2), 173–182.
- (11) Brezny, R.; Mihalov, V.; Kovacik, V. Low-temperature thermolysis of lignins. 1. Reactions of beta-o-4 model compounds. *Holzforschung* 1983, 37 (4), 199–204.
- (12) Asatryan, R.; Bennadji, H.; Bozzelli, J. W.; Ruckenstein, E.; Khachatryan, L. Molecular Products and Fundamentally Based Reaction Pathways in the Gas-Phase Pyrolysis of the Lignin Model Compound p-Coumaryl Alcohol. J. Phys. Chem. A 2017, 121 (18), 3352–3371.
- (13) Bridgwater, A. V.; Cottam, M. L. Opportunities for Biomass Pyrolysis Liquids Production and Upgrading. *Energy Fuels* 1992, 6 (2), 113–120.
- (14) Morf, P.; Hasler, P.; Nussbaumer, T. Mechanisms and kinetics of homogeneous secondary reactions of tar from continuous pyrolysis of wood chips. *Fuel* 2002, *81* (7), 843–853.
- (15) Barekati-Goudarzi, M.; Boldor, D.; Marculescu, C.; Khachatryan, L. The Peculiarities of Pyrolysis of Hydrolytic Lignin in Dispersed Gas Phase and in Solid State. *Energy Fuels* 2017, 31 (11), 12156–12167.
- (16) Shaub, W. H.; Bauer, S. H. Laser Powered Homogeneous Pyrolysis. IEEE J. Quantum Electron. 1975, 11 (8), 714-714.
- (17) Shaub, W. M.; Bauer, S. H. Laser-Powered Homogeneous Pyrolysis. Int. J. Chem. Kinet. 1975, 7 (4), 509-529.
- (18) Zitter, R. N. Nearly Thermalized Systems under Continuous Infrared-Laser Excitation Expected and Unexpected Effects. Spectrochimica Acta Part a-Molecular and Biomolecular Spectroscopy 1987, 43 (2), 245–251.
- (19) Kubat, P.; Pola, J. Spatial Temperature Distribution in Cw Co2-Laser Photosensitized Reactions. *Collect. Czech. Chem. Commun.* 1984, 49 (6), 1354–1359.
- (20) Molin, Y. N.; Panfilov, V. N.; Petrov, A. K. Infrared Photochemistry. *Novosibirsk, Izd. Nauka,* 1985.
- (21) Sukiasyan, A. A.; Khachatryan, L. A.; Il'in, S. D. Measuring of the kinetic parameters of homogeneous decomposition of Azomethane under CO<sub>2</sub>-laser irradiation. *Arm. Khim. Zhur.* 1988, 41, 104.
- (22) Russell, D. K. Infrared-Laser Powered Homogeneous Pyrolysis. Chem. Soc. Rev. 1990, 19 (4), 407–437.
- (23) Mantashyan, A. A.; Khachatryan, L. A.; Sukiasyan, A. A. An investigation of gas phase chain reactions of consumption of the hydrocarbon-oxygen mixtures under laser irradiation. *Revue Roumeine Chim.* 1989, 34, 821.
- (24) Smith, E. A.; Lee, Y. J. Petroleomic Analysis of Bio-oils from the Fast Pyrolysis of Biomass: Laser Desorption Ionization-Linear Ion Trap-Orbitrap Mass Spectrometry Approach. *Energy Fuels* 2010, 24, 5190–5198.
- (25) Velikyan, I. V.; Khachatryan, L. A.; Mantashyan, A. A. The peculiarities of oxidation of methane in the oxygen-rich mixtures under IR laser irradiation. *Khim. Phizika.* 1993, 12, 413.
- (26) Mantashyan, A. A.; Khachatryan, L. A.; Velikyan, I. V. The oxidation of methane under laser irradiation. *Khim. Phizika*. 1993, 12, 466.
- (27) Velikyan, I. V.; Khachatryan, L. A.; Mantashyan, A. A. Conversion of butane-oxygen mixture sensitised by SF6 under IR laser irradiation. *Chem. Phys. Rep.* 1994, 13, 330.
- (28) Mantashyan, A. A.; Khachatryan, L. A.; Sukiasyan, A. A.; Adilkhanyan, D. M.; Velikyan, I. V. Modeling of Homogeneous Reaction of Propane with Oxygen. *Khimicheskaya Fizika* 1994, 13 (10), 88–96.
- (29) Khachatryan, L.; Fajgar, R.; Haas, Y.; Pola, J. Laser-powered homogeneous decomposition of secondary butene-2-ozonide: the

evidence for intermediary of products of rearrangement. J. Chem. Soc., Perkin Trans. 2 1996, 2, 1981.

- (30) Khachatryan, L. A.; Russell, D. K.; Pola, J. An evidence of polymer radicals in the thermal decomposition of silacyclobutane on the surfaces under CW CO<sub>2</sub> laser irradiation, *Unpublished data*, 1999.
- (31) Samsonov, Y. N.; Petrov, A. K.; Baklanov, A. V. a.; Vihzin, V. V. Homogeneous decomposition of gaseous formic acid induced by a carbon dioxide laser. *React. Kinet. Catal. Lett.* 1976, 5 (2), 197–202.
- (32) Sugawara, K.; Nakanaga, T.; Takeo, H.; Matsumura, C. Diode-Laser Kinetic Measurements of Vibrational Rotational and Translational Temperatures of Co in Co2 Laser-Excited Sf6. *Chem. Phys.* 1989, 135 (2), 301–306.
- (33) Bauer, S. H. Laser-Heating for Chemical Conversions Unique Features and Limitations. Spectrochimica Acta Part a-Molecular and Biomolecular Spectroscopy 1987, 43 (2), 227–235.
- (34) Tsang, W. Single-Pulse Shock-Tube Studies on the Decomposition of 1,2-Dibromoperfluoroethane and Allyl Bromide. *J. Phys. Chem.* 1984, 88 (13), 2812–2817.
- (35) Gardon, R. The Emissivity of Transparent Materials. J. Am. Ceram. Soc. 1956, 39 (8), 278-287.
- (36) Watanabe, K.; Zelikoff, M.; Inn, E. C. Y.Absorption coefficients of several atmospheric gases. *Geophys. Res. Directorate* 1953, 21, 54–55
- (37) Znotins, T. A. Absorption Properties of SF<sub>6</sub> near 10.6  $\mu$ m, Open Access Dissertations and Theses, 1978.
- (38) Nowak, A. V.; Lyman, J. L. Temperature-Dependent Absorption-Spectrum of V3 Band of Sf6 at 10.6 Mum. J. Quant. Spectrosc. Radiat. Transfer 1975, 15 (10), 945-961.
- (39) Blackford, D. B.; Simons, G. R. Particle Size Analysis of Carbon Black. *Part. Part. Syst. Charact.* 1987, 4, 112–117.
- (40) Bährle, C.; Nick, T. U.; Bennati, M.; Jeschke, G.; Vogel, F. High-Field Electron Paramagnetic Resonance and Density Functional Theory Study of Stable Organic Radicals in Lignin: Influence of the Extraction Process, Botanical Origin, and Protonation Reactions on the Radical g Tensor. J. Phys. Chem. A 2015, 119 (24), 6475–82.
- (41) Nicholson, D. J.; Guilford, C. R.; Abiola, A. B.; Bose, S. K.; Francis, R. C. Estimation of the S/G ratios of the lignins in three widely used North American hardwoods. *Tappi J.* 2016, *15* (7), 449–457.
- (42) Lawson, J. R.; Klein, M. T. Influence of Water on Guaiacol Pyrolysis. Ind. Eng. Chem. Fundam. 1985, 24 (2), 203-208.
- (43) Asmadi, M.; Kawamoto, H.; Saka, S. Thermal reactions of guaiacol and syringol as lignin model aromatic nuclei. *J. Anal. Appl. Pyrolysis* 2011, 92 (1), 88–98.
- (44) Bai, X.; Kim, K. H.; Brown, R. C.; Dalluge, E.; Hutchinson, C.; Lee, Y. J.; Dalluge, D. Formation of phenolic oligomers during fast pyrolysis of lignin. *Fuel* 2014, 128, 170–179.
- (45) Liu, C.; Zhang, Y. Y.; Huang, X. L. Study of guaiacol pyrolysis mechanism based on density function theory. *Fuel Process. Technol.* 2014, 123, 159–165.
- (46) Huang, J. B.; Li, X. S.; Wu, D.; Tong, H.; Li, W. M. Theoretical studies on pyrolysis mechanism of guaiacol as lignin model compound. *J. Renewable Sustainable Energy* 2013, 5 (4), 043112.
- (47) Custodis, V. B.; Hemberger, P.; Ma, Z.; van Bokhoven, J. A. Mechanism of fast pyrolysis of lignin: studying model compounds. *J. Phys. Chem. B* 2014, 118 (29), 8524–31.
- (48) Van de Velden, M.; Baeyens, J.; Brems, A.; Janssens, B.; Dewil, R. Fundamentals, kinetics and endothermicity of the biomass pyrolysis reaction. *Renewable Energy* 2010, 35 (1), 232–242.
- (49) Micic, M.; Jeremic, M.; Radotic, K.; Mavers, M.; Leblanc, R. M. Visualization of artificial lignin supramolecular structures. *Scanning* 2000, 22 (5), 288–294.
- (50) Khachatryan, L.; Adounkpe, J.; Maskos, M.; Dellinger, B. Formation of Cyclopentadienyl Radicals from the Gas-Phase Pyrolysis of Hydroquinone, Catechol, and Phenol. *Environ. Sci. Technol.* 2006, 40, 5071–5076.
- (51) Khachatryan, L.; Adounkpe, J.; Dellinger, B. Formation of Phenoxy and cyclopentadienyl radicals from the gas-phase pyrolysis of phenol. *J. Phys. Chem. A* 2008, *112*, 481–487.

(52) Xu, C.; Ferdosian, F. Degradation of Lignin by Pyrolysis. In Conversion of Lignin into Bio-Based Chemicals and Materials; Springer: Berlin Heidelberg, 2017; pp 13–33.

(53) Mulholland, J. A.; Lu, M.; Kim, D. H. Pyrolytic growth of polycyclic aromatic hydrocarbons by clyclopentadienyl moieties. *Proc. Combust. Inst.* 2000, 28, 2593–2599.